A RESCALED V2-F MODEL: FIRST APPLICATION TO SEPARATED AND IMPINGING FLOWS

R. Manceau, Sabrina Carpy, D. Alfano

A RESCALED $\overline{v^2}$–f MODEL: FIRST APPLICATION TO SEPARATED AND IMPINGING FLOWS

R. Manceau, S. Carpy and D. Alfano

Laboratoire d'études aérodynamiques, UMR CNRS 6609, université de Poitiers, SP2MI, téléport 2, bd Marie et Pierre Curie, BP 30179, 86962 Futuroscope Chasseneuil, France

ABSTRACT

The ability of the rescaled version of the $\overline{v^2}$–f model, designed to improve the predictions in channel flows, to reproduce pressure driven separation and impinging flows is investigated. First, it is shown that the recalibration of the coefficients does not suppress the gain obtained previously in channel flows concerning the prediction of the mean velocity and $\overline{v^2}$ profiles, and the evolution of the friction coefficient with the Reynolds number. The original and rescaled $\overline{v^2}$–f models are then applied to a plane asymmetric diffuser and an impinging jet, which are known for being well reproduced by the original model. The rescaled model globally gives very similar results in these flows. However, room for improvement exists in predicting the reattachment region in the diffuser and the Nusselt number distribution in the impinging jet.

KEYWORDS

Near-wall RANS turbulence models, elliptic relaxation, channel flow, plane asymmetric diffuser, impinging jet.

INTRODUCTION

The elliptic relaxation approach, initially proposed by Durbin [6, 7], is now widely accepted as an efficient way to reproduce the blocking effect of solid boundaries on turbulence. When applied to the standard k–ε model, it leads to the $\overline{v^2}$–f model which can be integrated down to solid boundaries and has proven to give accurate predictions in a range of flows: separated flows [8, 10, 14], impinging jets [2, 3, 17], 3D boundary layers [18], etc.

However, the main weakness of this model, as well as of second moment closures using the elliptic relaxation strategy, is the inaccurate prediction of the log layer in channel flows. This has been the motivation for a series of studies during the past decade [21, 15, 13] that all led to the conclusion that modifying the elliptic relaxation operator $(1 - L^2\nabla^2)$ can allow overcoming the problem.

Recently, Manceau *et al.* [12] proposed a different modification that does not consist in altering the elliptic operator but in applying the methodology to the non-dimensional redistribution term ϕ_{ij}/ε (where ε is the turbulent energy dissipation rate) instead of the redistribution term ϕ_{ij} itself. This minor change in the model induces a significant improvement of the predictions in a channel flow over a wide range of Reynolds numbers that cannot be obtained by simply recalibrating the coefficients of the original model [12].

In the present paper, this new formulation (called hereafter the *rescaled* $\overline{v^2}$*–f model*) is applied to test cases involving flow regimes that underly a wide range of flows of industrial interest: boundary layer separation under adverse pressure gradient and impinging flows. The asymmetric plane diffuser [4] and the impinging jet [5, 1] are chosen because previous studies [8, 2] showed that these flows can be well reproduced by the original $\overline{v^2}$–f model. The purpose of the present work is then to show that the rescaled $\overline{v^2}$–f model, which improves the predictions in channel flows, behaves at least as well as the original $\overline{v^2}$–f model in the different flows quoted above. In other words, the present work can be considered a calibration process, based on three different type of flows (including the channel flow at different Reynolds numbers).

PRESENTATION OF THE RESCALED MODEL

The equations of the original $\overline{v^2}$–f model and of the rescaled model are those used by Parneix *et al.* [18] and Manceau *et al.* [12], respectively. Note that in both models, a realizability constraint [2] is applied on the turbulent time and length scales (with the coefficient $\alpha = 0.6$). Both models can be written in the general form:

$$\frac{Dk}{Dt} = P - \varepsilon + \frac{\partial}{\partial x_j}\left[\left(\nu + \frac{\nu_t}{\sigma_k}\right)\frac{\partial k}{\partial x_j}\right] \tag{1}$$

$$\frac{D\varepsilon}{Dt} = \frac{1}{T}\left(C'_{\varepsilon 1}P - C_{\varepsilon 2}\varepsilon\right) + \frac{\partial}{\partial x_j}\left[\left(\nu + \frac{\nu_t}{\sigma_\varepsilon}\right)\frac{\partial \varepsilon}{\partial x_j}\right] \tag{2}$$

$$\frac{D\overline{v^2}}{Dt} = \xi k f_{22} - \frac{\overline{v^2}}{k}\varepsilon + \frac{\partial}{\partial x_j}\left[\left(\nu + \frac{\nu_t}{\sigma_k}\right)\frac{\partial \overline{v^2}}{\partial x_j}\right] \tag{3}$$

$$f_{22} - L^2\nabla^2 f_{22} = (C_1 - 1)\frac{2/3 - \overline{v^2}/k}{\xi T} + \frac{2}{3}C_2\frac{P}{\xi k} \tag{4}$$

$$\nu_t = C_\mu \overline{v^2} T \quad ; \quad T = \max\left[\frac{k}{\varepsilon}; C_T\sqrt{\frac{\nu}{\varepsilon}}\right]; \quad L = C_L \max\left[\frac{k^{3/2}}{\varepsilon}; C_\eta\left(\frac{\nu^3}{\varepsilon}\right)^{1/4}\right] \tag{5}$$

$$C'_{\varepsilon 1} = C_{\varepsilon 1}\left[1 + A_1\left(\frac{k}{\overline{v^2}}\right)^{1/2}\right] \tag{6}$$

where $\xi = 1$ for the original model and $\xi = \varepsilon$ for the rescaled model.

These equations are then solved subject to the boundary conditions at solid boundaries:

$$k = 0 \quad ; \quad \varepsilon = \frac{2\nu k}{y^2} \quad ; \quad \overline{v^2} = 0 \quad ; \quad f_{22} = -\frac{20\nu^2\overline{v^2}}{\xi\varepsilon y^4} \tag{7}$$

The terms in the rescaled model that differ from those of the original model are pointed out here:

- The redistribution term ϕ_{22} in the $\overline{v^2}$ transport equation is modelled by $\phi_{22} = \varepsilon k f_{22}$ instead of $\phi_{22} = k f_{22}$.

- Consequently, the source term of the elliptic relaxation equation satisfied by f_{22} is $\Pi_{22}/\varepsilon k$ (where Π_{22} is the 22-component of the Launder *et al.* [11] redistribution model) instead of Π_{22}/k.

- The boundary condition satisfied by f_{22} at solid boundaries is $f_{22} = -20\nu^2\overline{v^2}/\varepsilon^2 y^4$ instead of $f_{22} = -20\nu^2\overline{v^2}/\varepsilon y^4$.

- The coefficients of the rescaled model have been calibrated during the present study by means of the rudimentary but efficient technique of trials and errors, while keeping the coefficients corresponding to the high-Reynolds number k–ε model as close as possible to their standard values: basically, only the coefficients C_L, C_η and A_1 provide some degrees of freedom. Since the set of coefficients differs from that used by Manceau *et al.* [12], the channel flows investigated in the latter paper have been computed again and the results are given in the following section in order to show that the recalibration does not suppress the improvement obtained previously. All the results presented below for the rescaled model are thus obtained with the following set of coefficients:

$$\begin{gathered} C_\mu = 0.22 \ ; \ \sigma_k = 1 \ ; \ \sigma_\varepsilon = 1.3 \ ; \ C_{\varepsilon 1} = 1.44 \ ; \ C_{\varepsilon 2} = 1.91 \ ; \\ C_1 = 1.8 \ ; \ C_2 = 0.4 \ ; \ C_L = 0.23 \ ; \ C_\eta = 100 \ ; \ A_1 = 0.06 \ ; \ \alpha = 0.6 \end{gathered} \tag{8}$$

  The coefficients of the original $\overline{v^2}$–f model are

$$\begin{gathered} C_\mu = 0.22 \ ; \ \sigma_k = 1 \ ; \ \sigma_\varepsilon = 1.3 \ ; \ C_{\varepsilon 1} = 1.4 \ ; \ C_{\varepsilon 2} = 1.9 \ ; \\ C_1 = 1.4 \ ; \ C_2 = 0.3 \ ; \ C_L = 0.25 \ ; \ C_\eta = 85. \ ; \ A_1 = 0.045 \ ; \ \alpha = 0.6 \end{gathered} \tag{9}$$

  Note that one of the main differences between the two models is that the rescaled approach allows the use of the standard coefficients C_1 and C_2 of the Launder *et al.* [11] model (the value $C_2 = 0.4$ corresponds to the original $C_2 = 0.6$, the definitions differing by a factor of 2/3), while the original $\overline{v^2}$–f model uses much lower values.

CHANNEL FLOWS

The available set of direct numerical simulation data at different friction Reynolds numbers Re_τ ($Re_\tau = 180$, 395 and 590 [16]), as well as the experimental results of Wei and Willmarth [19, 20] at $Re_\tau = 1017$ are used to assess the improvement induced by the new scaling of ϕ_{22}. A simple finite difference 1D code is used with second order discretization, which allows to impose Re_τ through a scaling of the equations by u_τ (friction velocity) and h (half-width of the channel).

Results obtained with the original and rescaled formulations of the $\overline{v^2}$–f model are presented in Fig. 1 and compared with the DNS and experimental data. It can be seen in Fig. 1a that the mean velocity profiles are significantly better predicted by the rescaled model. It is worth pointing out that the rescaled model is more sensitive to the reduction of the Reynolds number, with no other modification than the rather natural scaling of ϕ_{22} by ε. This feature is illustrated by Fig. 2, where the evolution of the friction coefficient $C_f = 2u_\tau^2/U_c^2$ with the Reynolds number $Re_c = U_c h/\nu$ is plotted (U_c: centreline velocity).

The corresponding $\overline{v^2}$ profiles are shown in Fig. 1c. The rescaled model better predicts the entire y^+ distribution, including the peak, over the Reynolds number range examined. A major improvement is obtained in the central region of the flow, in particular at the lowest Reynolds number. Fig. 1b shows that the rescaled model generally under-predicts the turbulent energy (no experimental

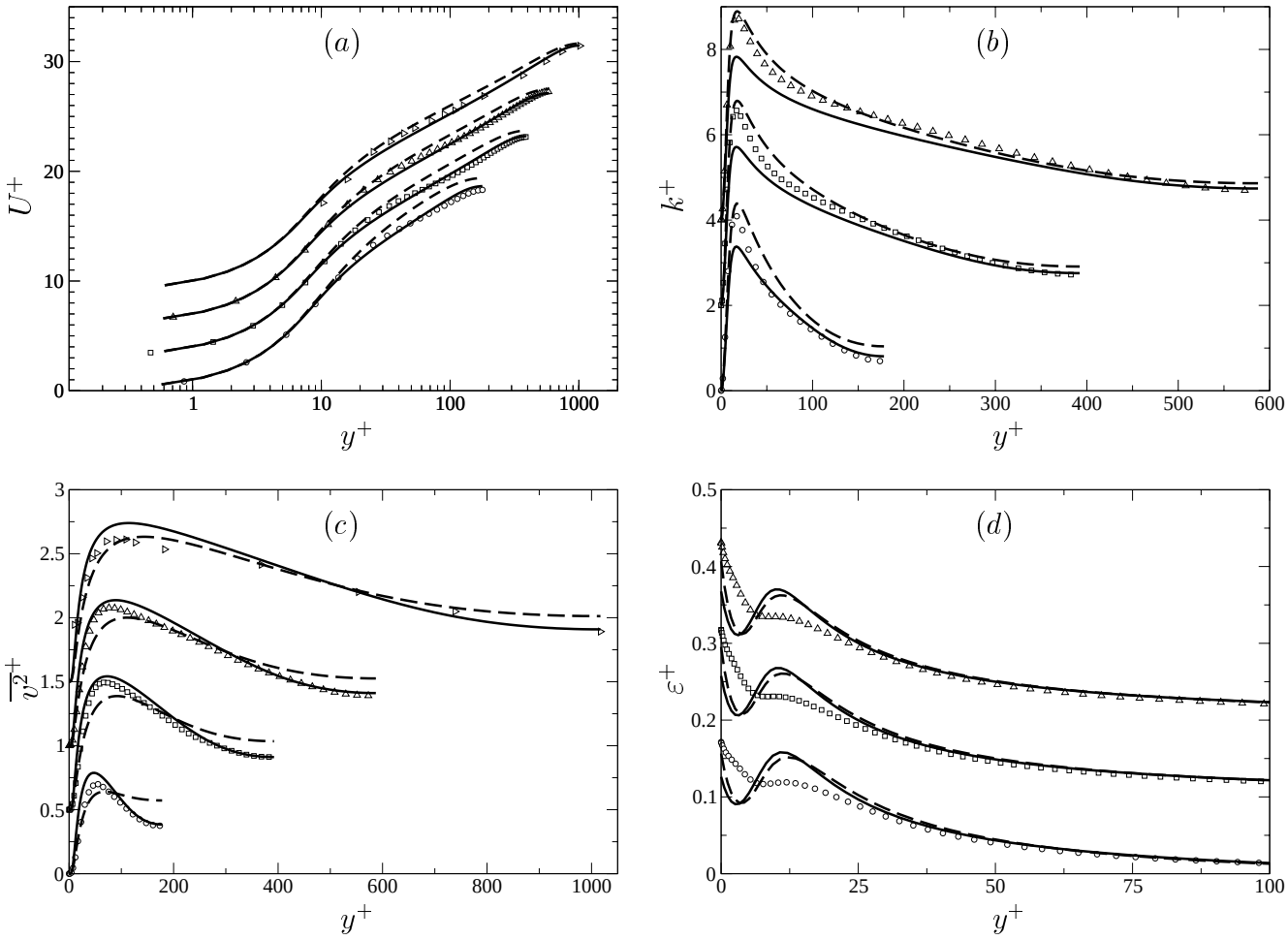

Figure 1: Profiles obtained with the two formulations of the $\overline{v^2}$–f model in a channel flow at different Reynolds numbers: (a) Mean velocity U; (b) Turbulent energy k; (c) Wall-normal Reynolds stress $\overline{v^2}$; (d) Dissipation rate ε. Symbols: DNS data [16] at $Re_\tau = 180$ (○), $Re_\tau = 395$ (□) and $Re_\tau = 590$ (△), and experimental data [19, 20] at $Re_\tau = 1017$ (▷). Lines: predictions of the original $\overline{v^2}$–f model (– – –) and of the rescaled $\overline{v^2}$–f model (——).

data are available at $Re_\tau = 1017$). However, it is again worth noting that the central region of the channel is much better reproduced. Consequently, at $Re_\tau = 180$, the y^+ distribution is globally better predicted by the rescaled model, since the central region has a very strong influence over the whole flow at this low Reynolds number. The under-estimation of the peak of turbulent energy is more significant than in Manceau *et al.* [12], because of the recalibration of the coefficients, which has been necessary to improve the prediction of the flow in the plane asymmetric diffuser presented in the next section.

From Figs. 1 and 2, it is clear that the rescaled model globally improves the prediction of the channel flow, over the range of Reynolds numbers investigated in the present work, in particular regarding the prediction of the friction coefficient and of the turbulent quantities (k and $\overline{v^2}$) at the centre. As presented in Manceau *et al.* [12], this can be related to the scaling of ϕ_{22} by ε: since the source term of the elliptic relaxation equation is basically constant away from the wall, the elliptic operator is "neutral" in this region (i.e., does not amplify nor reduce the redistribution) and is only active in the very-near-wall region (sub- and buffer layer), which avoids undesired side effects in the log layer.

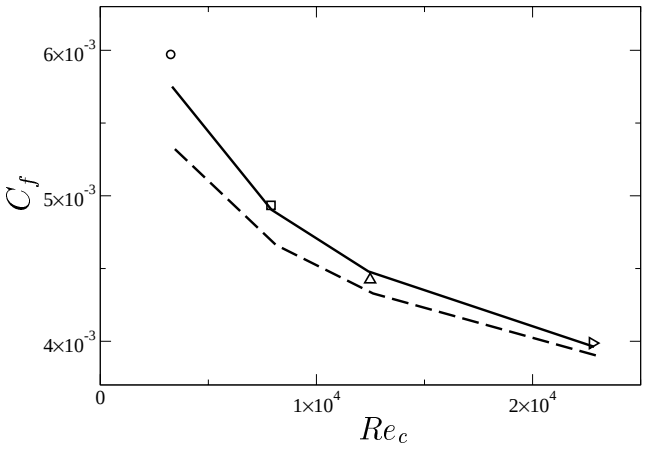

Figure 2: Channel flow: variation of the friction coefficient $C_f = 2u_\tau^2/U_c^2$ with the centreline Reynolds number $Re_c = U_c h/\nu$. Symbols: DNS data [16] at $Re_\tau = 180$ (○), $Re_\tau = 395$ (□) and $Re_\tau = 590$ (△), and experimental data [19, 20] at $Re_\tau = 1017$ (▷). Lines: predictions of the original $\overline{v^2}$–f model (– – –) and of the rescaled $\overline{v^2}$–f model (——).

PLANE ASYMMETRIC DIFFUSER

The experimental database of Buice and Eaton [4] is used to evaluate the ability of the rescaled $\overline{v^2}$–f model to reproduce the flow in a plane asymmetric diffuser after proper calibration. In this flow, the expansion ratio of 4.7 is sufficient to produce a strong pressure gradient which causes separation. The shape of the lower, sloping wall is smooth, such that the location of the separation point is not fixed by the geometry but driven by the pressure gradient. The Reynolds number is $Re_c = 20,000$, based on the centreline velocity U_c and the upstream channel height H. The sloping wall is inclined by 10 degrees and is $21.3H$ long.

The commercial package Star-CD is used, the two versions of the $\overline{v^2}$–f model being implemented via user subroutines. The code uses finite volumes, with second order discretization. The SIMPLE algorithm and a central differencing scheme (second order) for the convection terms are used. The grid consists of $90 \times 220 \times 1$ hexahedra. The cells are clustered near the wall such that the first calculation nodes are located at $x_n^+ < 1$. The inlet boundary is located $12H$ before the beginning of the sloping wall. The inlet boundary conditions are generated by a separate channel flow computation with the 1D code used in previous section. The outlet is located $100H$ after the end of the sloping wall.

Fig. 3 shows the mean velocity U (inflow direction) profiles at different locations obtained with the two versions of the $\overline{v^2}$–f model. Fig. 3a confirms that the original model is able to predict quite satisfactorily the smooth separation occurring in this flow [8]. However, it can be seen in Figs. 3c and 4 that the reattachment occurs slightly too early and that the intensity of the backflow is underestimated: this causes an underestimation of the mean velocity close to the upper wall (Fig. 3a) as a consequence of mass conservation.

It is clear from Fig. 3a that the rescaling of the elliptic relaxation equation does not spoil the predictions of the model in this flow, since solid and dashed curves are almost indistinguishable. However, Figs. 3b, 3c and 4 show some discrepancies between the two versions of the model. In Fig. 3b, it is observed that the shape of the mean velocity U in the very-near-wall region is slightly better reproduced by the rescaled model, at the two locations ($x/H = 2.59$ and $x/H = 5.98$) shown in the figure: the original model underestimates the mean velocity, which leads to a slightly too early separation, as shown in Fig. 4; the rescaled model predicts a slightly too late separation

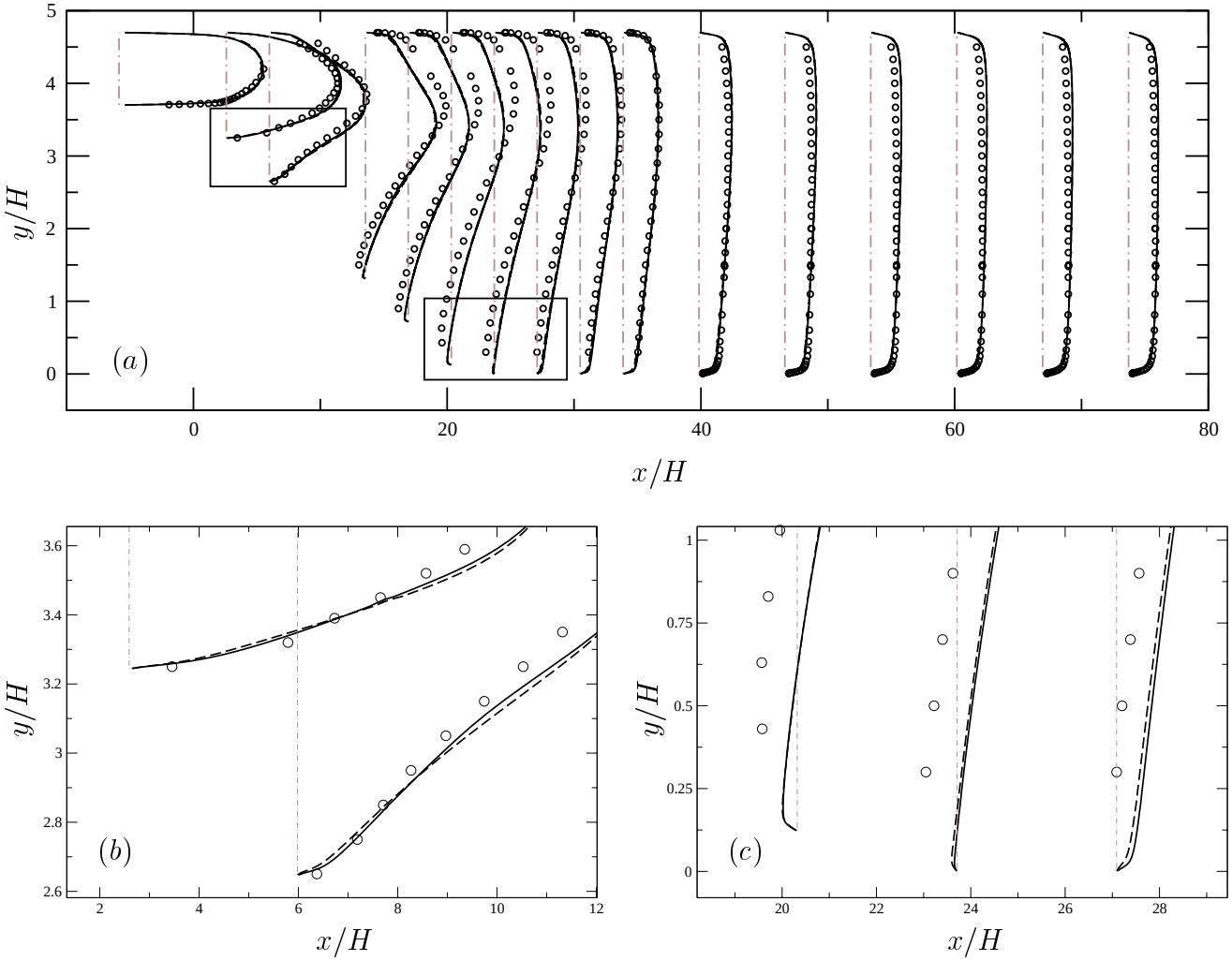

Figure 3: Profiles of the U-component of the mean velocity obtained with the two formulations of the $\overline{v^2}$–f model in a plane asymmetric diffuser: ○ Experimental data [4]; – – – Original $\overline{v^2}$–f model; —— Rescaled $\overline{v^2}$–f model. (b) and (c) are detailed views corresponding to the boxes plotted in (a).

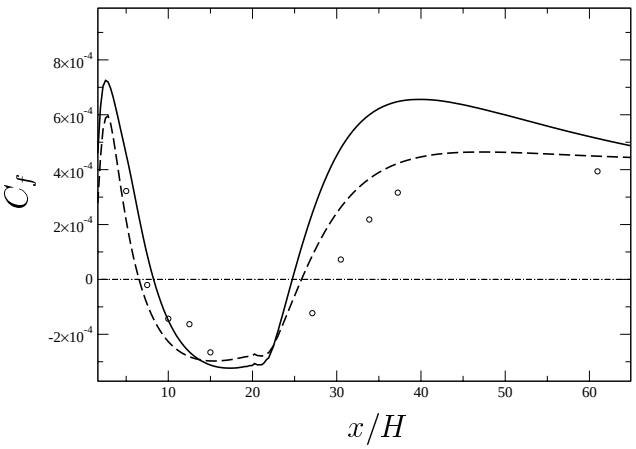

Figure 4: Plane asymmetric diffuser: friction coefficient $C_f = 2u_\tau^2/U_b^2$ predicted by the two versions of the $\overline{v^2}$–f model. ○ Experimental data [4]; – – – Original $\overline{v^2}$–f model; —— Rescaled $\overline{v^2}$–f model.

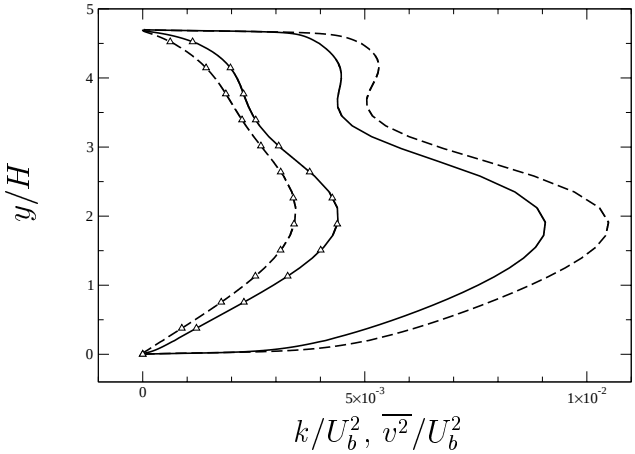

Figure 5: Plane asymmetric diffuser: k and $\overline{v^2}$ profiles at the location $x/H = 23.71$. Original $\overline{v^2}$–f model: – – – k; △– – –△ $\overline{v^2}$. Rescaled $\overline{v^2}$–f model: —— k; △——△ $\overline{v^2}$.

despite a better prediction of the mean velocity at $x/H = 5.98$.

It can be seen in Fig. 3c that the two models give almost exactly the same underestimated backflow at $x/H = 20.32$, but that the original model reattaches slightly latter than the rescaled model: this is emphasized in Fig. 4 which shows that the rescaled model predicts too sharp an increase of the friction coefficient in the reattachment region. This difference compared to the original model may be related (the lack of experimental data does not allow to draw definitive conclusions) to an overestimation of the turbulent viscosity $\nu_t = C_\mu \overline{v^2} T$ in the near wall region (not shown here), due to a high level of $\overline{v^2}$, shown in Fig. 5, which is not fully compensated by the low level of k (recall that $T = \max[k/\varepsilon; 6(\nu/\varepsilon)^{1/2}]$). This result is consistent with what is observed in a channel flow (Figs. 1b and c). Note that the original model strongly underestimates $\overline{v^2}$ in channel flows (Fig. 1c) and overestimates k (Fig. 1b). The same tendency is observed in Fig. 5 by comparing the two models: by compensation of errors, the original model may eventually lead to a better prediction of the turbulent viscosity. This overestimation of $\overline{v^2}$ by the rescaled model is a consequence of too weak a blocking effect of the wall: this can be corrected by increasing the coefficient C_L, but this has the undesirable side effect of delaying the separation on the sloping wall. Further investigations are necessary to understand how to reconcile these two aspects.

IMPINGING JET

The Cooper *et al.*. [5] and Baughn and Shimizu [1] databases, containing respectively flow field and heat transfer measurements, are used to assess the ability of the rescaled model to predict impinging jets, which are known for being very well reproduced by the original $\overline{v^2}$–f model [2, 3, 17]. The configuration chosen for the present study consists of an air jet (Prandtl number $Pr = 0.71$) at the ambient temperature T_0 issuing from a circular pipe of diameter D with the bulk velocity U_b and impinging on a heated flat plate (constant heat flux $\dot{q}_w$) located at the distance $H = 2D$ from the pipe exit.

The numerical method is the same as in previous section. This axisymmetric problem is solve in a 5 degree sector with symmetry boundary conditions in the azimuthal direction. The grid consists of $150 \times 120 \times 1$ hexahedra with a strong clustering near all the walls such that the first calculation nodes are located below $x_n^+ = 1$. The inlet boundary conditions are applied $2D$ before the pipe exit and are evaluated from a separate developed pipe flow computation. The turbulent heat fluxes are modelled by a turbulent diffusivity hypothesis, with a constant turbulent Prandtl number $Pr_t = 0.9$.

Fig. 6 shows the mean velocity magnitude predicted by the two versions of the $\overline{v^2}$–f model close to the plate compared to the experimental data of Cooper *et al.* [5]. It is clear from this figure that both model are in very good agreement with the data. Two regions can however be distinguished, separated by the horizontal line $x/D = 0.1$. In the first region ($x/D > 0.1$), the rescaled model is in closer agreement to the data than the original model at every r/D location, except for $r/D = 0.5$, where the two predictions are basically identical; in the second region ($x/D < 0.1$), the rescaled model gives slightly better predictions at two locations ($r/D = 0$ and $r/D = 1$), but leads to a slight overestimation of the velocity at the other locations.

Fig. 7 shows the evolution of the Nusselt number $Nu = \dot{q}_w D/\kappa(T_w - T_0)$ along the heated plate. It can be observed that the prediction of the rescaled model after $r/D \simeq 2.5$ is very similar to that of the original model, and is lower than the experimental value. In the impingement region, the rescaled model gives significantly lower values than the original model. Both models are unable to reproduce the second maximum located around $r/D = 2$, which is consistent with the results found by Behnia *et al.* [2]. The discrepancy between the two models can be traced to the prediction of k and $\overline{v^2}$ along the stagnation line, which is plotted in Fig. 8. Indeed, it is observed that the

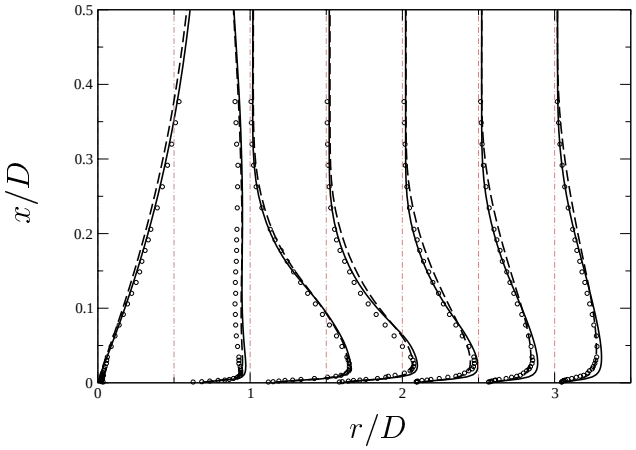

Figure 6: Impinging jet: mean velocity magnitude close to the plate. ○ Experimental data [5]; – – – Original $\overline{v^2}$–f model; —— Rescaled $\overline{v^2}$–f model.

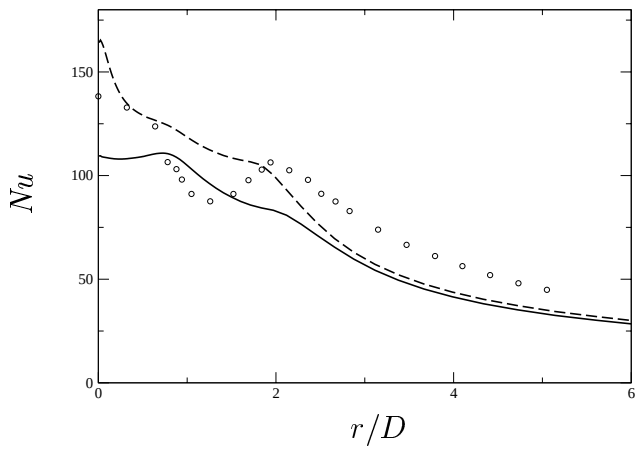

Figure 7: Impinging jet: evolution of the Nusselt number $Nu = \dot{q}_w D/\kappa(T_w - T_0)$ along the heated plate. ○ Experimental data [1]; – – – Original $\overline{v^2}$–f model; —— Rescaled $\overline{v^2}$–f model.

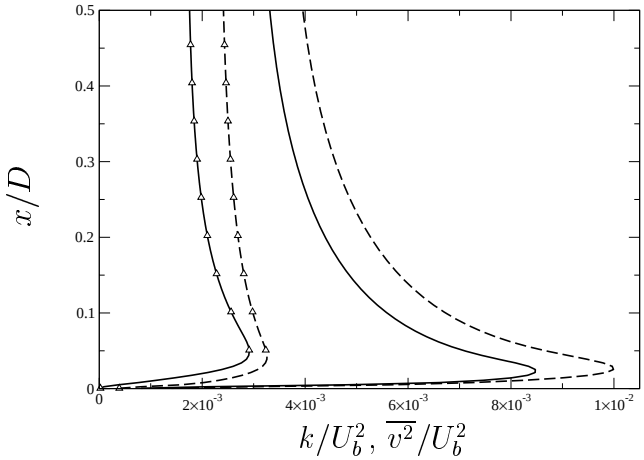

Figure 8: Impinging jet: k and $\overline{v^2}$ profiles at the location $r/D = 0$. Original $\overline{v^2}$–f model: – – – k; △– – –△ $\overline{v^2}$. Rescaled $\overline{v^2}$–f model: —— k; △——△ $\overline{v^2}$.

values predicted by the rescaled model are lower than those predicted by the original model, for both k and $\overline{v^2}$: it results in lower levels of turbulent viscosity in the impingement region, and, in turn, of turbulent diffusivity. Fig. 8 shows that these low levels are also present upstream (further from the plate), which suggests that they may be inherited from the pipe flow centre, where, similarly to the centre of the channel flow (Figs. 1b–c), the rescaled model predicts lower values of k and $\overline{v^2}$ than the original model. However, it is worth noting that even though it can explain the difference between the two models, it does not justify the underestimation of the Nusselt number by the rescaled model.

CONCLUSION

The present study was devoted to the investigation of the ability of the rescaled $\overline{v^2}$–f model proposed by Manceau *et al.* [12] to reproduce correctly three types of flows: developed channel flows, flows with strong pressure gradient causing separation and impinging flows. The six selected test cases (channel flow at four Reynolds numbers, plane asymmetric diffuser, impinging jet) allowed the calibration of the set of coefficients in order to reach a compromise enabling the

prediction of the main characteristics of the different flows: evolution of the friction coefficient with the Reynolds number for the channel flow; separation location and recirculation length for the diffuser flow; Nusselt number for the impinging jet.

The main consequence of the rescaling of the elliptic relaxation equation is the improvement of the channel flow predictions, as shown by Manceau *et al.* [12]: the overestimation of the mean velocity is suppressed; the friction coefficient and its evolution with the Reynolds number are much closer to DNS and experiments; the spurious shape of $\overline{v^2}$ in the centre of the channel disappears. The present study showed that this series of improvements is not spoiled by the recalibration of the coefficients.

In the diffuser case, the mean velocity field predicted by the rescaled model is very close to that predicted by the original model. However, the reattachment occurs slightly earlier and the friction coefficient experiences a steeper increase in the reattachment region. This is believed to be due to a too weak blocking effect of the wall, driven by the C_L coefficient: unfortunately, increasing this coefficient has the side effect of delaying the separation on the sloping wall.

The impinging flow is very well predicted by both versions of the model, and the results are very close to each other. However, the Nusselt number in the impingement region is slightly overestimated by the original model, and underestimated by the rescaled model. This discrepancy is believed to be related to the predictions in the centre of the inlet pipe flow.

Further investigations are necessary to understand the role of the blocking effect in the crucial regions of the flow: separation and reattachment regions for the diffuser; impingement region for the jet. Indeed, it appears, through comparisons of the predictions by the two models, that possible failures in some of these regions in reproducing the "blocked" turbulent scale $\overline{v^2}$, together with the turbulent energy, may be at the origin of the underestimation by the rescaled model of the recirculation length in the diffuser and of the Nusselt number in the impinging jet.

ACKNOWLEDGEMENTS

Authors are grateful to G. Iaccarino for providing the user subroutines for the implementation of the original $\overline{v^2}$–f model in the commercial package Star-CD. For details, see [9].

REFERENCES

[1] J. Baughn and S. Shimizu. Heat transfer measurements from a surface with uniform heat flux and an impinging jet. *J. Heat Transfer*, 111:1096–1098, 1989.

[2] M. Behnia, S. Parneix, and P. Durbin. Prediction of heat transfer in a jet impinging on a flat plate. *Intl J. Heat Mass Transfer*, 41(12):1845–1855, 1998.

[3] M. Behnia, S. Parneix, Y. Shabany, and P. A. Durbin. Numerical study of turbulent heat transfer in confined and unconfined impinging jets. *Intl J. Heat and Fluid Flow*, 20(1):1–9, 1999.

[4] C. U. Buice and J. K. Eaton. Experimental investigation of flow through an asymmetric plane diffuser. Technical Report No. TSD–107, Thermosciences Division, Department of Mechanical Engineering, Stanford University, Stanford, CA, USA, 1997.

[5] D. Cooper, D. C. Jackson, B. E. Launder, and G. X. Liao. Impinging jet studies for turbulence model assessment—I. Flow-field experiments. *Intl J. Heat Mass Transfer*, 36(10):2675–2684, 1993.

[6] P. A. Durbin. Near-wall turbulence closure modeling without "damping functions". *Theoret. Comput. Fluid Dynamics*, 3:1–13, 1991.

[7] P. A. Durbin. A Reynolds stress model for near-wall turbulence. *J. Fluid Mech.*, 249:465–498, 1993.

[8] P. A. Durbin. Separated flow computations with the k–ε–$\overline{v^2}$ model. *AIAA J.*, 33:659–664, 1995.

[9] G. Iaccarino. Predictions of a turbulent separated flow using commercial CFD codes. *Journal of Fluids Engineering*, 123(4):819–828, 2001.

[10] S. H. Ko. Application of a Reynolds stress model to separating boundary layers. In *Ann. Res. Briefs*, pages 199–211. Center for Turbulence Research, Stanford University, 1992.

[11] B. E. Launder, G. J. Reece, and W. Rodi. Progress in the development of a Reynolds-stress turbulence closure. *J. Fluid Mech.*, 68(3):537–566, 1975.

[12] R. Manceau, J. R. Carlson, and T. B. Gatski. A rescaled elliptic relaxation approach: neutralizing the effect on the log layer. *Submitted to Phys. Fluids*, 2002.

[13] R. Manceau and K. Hanjalić. A new form of the elliptic relaxation equation to account for wall effects in RANS modelling. *Phys. Fluids*, 12(9):2345–2351, 2000.

[14] R. Manceau, S. Parneix, and D. Laurence. Turbulent heat transfer predictions using the $\overline{v^2}$–f model on unstructured meshes. *Intl J. Heat and Fluid Flow*, 21(3):320–328, 2000.

[15] R. Manceau, M. Wang, and D. Laurence. Inhomogeneity and anisotropy effects on the redistribution term in Reynolds-averaged Navier–Stokes modelling. *J. Fluid Mech.*, 438:307–338, 2001.

[16] R. D. Moser, J. Kim, and N. N. Mansour. Direct numerical simulation of turbulent channel flow up to $Re_\tau = 590$. *Phys. Fluids*, 11(4):943–945, 1999.

[17] S. Parneix, M. Behnia, and P. A. Durbin. Predictions of turbulent heat transfer in an axisymmetric jet impinging on a heated pedestal. *J. Heat Transfer*, 120:1–7, 1998.

[18] S. Parneix, P. A. Durbin, and M. Behnia. Computation of 3D turbulent boundary layers using the $\overline{v^2}$–f model. *Flow, Turb. and Comb.*, 60:19–46, 1998.

[19] T. Wei and W. W. Willmarth. Reynolds-number effects on the structure of a turbulent channel flow. *J. Fluid Mech.*, 204:57–95, 1989.

[20] T. Wei and W. W. Willmarth. PCH12: Fully developed turbulent channel flow experiments. In *A Selection of Test Cases for the Validation of Large-Eddy Simulations of Turbulent Flows*, AGARD AR 345, 1998.

[21] V. Wizman, D. Laurence, M. Kanniche, P. Durbin, and A. Demuren. Modeling near-wall effects in second-moment closures by elliptic relaxation. *Intl J. Heat and Fluid Flow*, 17(3):255–266, 1996.